Defence Science Journal, Vol. 72, No. 2, March 2022, pp. 258-267, DOI : 10.14429/dsj.72.17371

Experimental Investigation of Peak Temperature and Microhardness in Friction Stir Processing of AA6082-T6 using Taguchi GRA

Jainesh Sarvaiya and Dinesh Singh*

Department of Mechanical Engineering, Sardar Vallabhbhai National Institute of Technology, Surat - 395 007, India

**E-mail: dineshsinghmed@gmail.com*

ABSTRACT

Friction stir processing demonstrated tremendous potential for improving mechanical properties and its success relies on the optimal level of process parameters that result in a flawless stir zone. The present study is an experimental investigation of performance characteristics peak temperature and microhardness on FSPed AA6082-T6. The experiments are designed using the Taguchi L16 orthogonal array by considering four different levels of rotational speed, traverse speed, shoulder diameter, and tilt angle. The grey relational analysis is used for multiple responses to optimise the FSP process parameters and analysis of variance is utilised to establish the relevance of parameters for these responses. According to the findings, the shoulder diameter and traverse speed are the most important determinants for peak temperature and microhardness. It is observed from the experimental analysis that the main reasons for defect formation are either excessive or inadequate heat generation. The multi-response optimal condition is attained at a rotating speed of 1400 rpm, transverse speed of 112 mm/min, shoulder diameter of 25 mm, and tilt angle of 1º.

Keywords: Friction stir processing; Peak temperature, Microhardness; Taguchi- Grey relational analysis; Analysis of variance

NOMENCLATURE

FSP	:	Friction Stir Processing
FSPed	:	Friction Stir Processed
GRA	:	Grey Relational Analysis
TRS	:	Tool Rotational Speed
TTS	:	Traverse Speed
TSD	:	Tool Shoulder Diameter
TTA	:	Tool Tilt Angle
T1-AS	:	Peak Temperature on Advancing Side
T2-RS	:	Peak Temperature on Retreating Side
ANOVA	:	Analysis of Variance
S/N ratio	:	Signal to Noise Ratio
GRG	:	Grey Relational Grade
GRC	:	Grey Relational Coefficient

1. INTRODUCTION

Friction stir processing (FSP) is a solid-state process that operates on a similar principle to friction stir welding and has shown excellent improvement in microstructure, mechanical, corrosive and tribological properties. FSP is a promising revolutionary technique that has applications in various fields, including altering or obtaining desired surface qualities, grain refinement, crack repair, removing casting defects and many more. Moreover, FSP is a green manufacturing process that produces no fumes, toxic gases, and radiation, and thus there is no adverse effect on the environment[1]. The aluminium alloys are extensively used in aerospace, transportation, and marine industries because of their unique properties like high strength to weight ratio, high thermal conductivity and corrosion resistance[2]. However, they lack hardness and wear resistance[3], which can be overcome either by microstructure modification or by incorporating reinforcing particles, which is possible through the FSP. In FSP, a high-strength tool penetrates the work material through stirring action and severe plastic deformation occurs in work material due to intense forces resulting in heat generation[1]. Therefore, the combined effect of the severe plastic deformation and the heat generation leads to fine or ultrafine grain microstructure, which improves the material properties[4-5]. Due to the solid-state nature of the FSP process, it eliminates all the defects that generally occur in fusion-based processes, such as oxidation, porosity, distortion, and the formation of detrimental phases[4]. The fusion method requires very high energy consumption and is challenging to regulate process parameters accurately. However, a few defects like a tunnel, cracks, kissing bonds, and pinholes are also observed in FSP due to insufficient heat generation or improper process parameters level[6-7].

Various researchers studied the influence of process parameters on the peak temperature and mechanical properties. Patel[8], *et al.* have achieved sound friction stir processed (FSPed) samples by lowering the processing temperature through active cooling techniques such as compressed air, water, and CO_2. They found that CO_2 gas cooling provided the highest

Received : 2 August 2021, Revised : 7 January 2022
Accepted : 11 February 2022, Online published : 11 May 2022

cooling rate and obtained a very fine grain microstructure. Chaudhary[9], *et al.* confirmed through statistical analysis in friction stir welding that the tilt angle is the most influential factor for the peak temperature compared to tool rotational speed and traverse speed. Additionally, they also noticed that during friction stir welding, the flow of material between the advancing and retreating sides is very complex, resulting in an uneven temperature, strain and strain rate distribution. The peak temperature on the advancing side remains higher than the retreating side. Wahid[10], *et al.* also witnessed a similar phenomenon during underwater friction stir welding of AA6082-T6 alloy. As a result, grain size on the advancing side is usually growing bigger as compared to the retreating side.

Researchers utilised several techniques to predict peak temperature and mechanical properties in FSP. Yousefpour[11], *et al.* investigated that a higher strain rate and higher peak temperature increase the dissolution of secondary phase particles during FSP. Cartigueyen and Mahadevan[12], have successfully developed mathematical regression models for predicting heat generation and experimented using the response surface method while taking peak temperature and microhardness into account for the fabrication of surface composites via FSP. The rise in peak temperature is observed if tool rotational speed increases, whereas it decreases with the increase in transverse speed and tilt angle. An increase in heat input reduces the cooling rate, providing extra time for grain growth, leading to coarser grain formation and vice-versa. Thus, peak temperature plays a vital role in deciding the microstructural characteristic of FSPed surface composites. Stringham[13], *et al.* have developed a non-dimensional empirical model for the rise in peak temperature and cooling time of heat-affected zone with R-squared (R^2) values of 0.997 and 0.995, respectively, for friction stir welding AA7075-T7351 and HSLA-65 using experimental designed data. This experimental design data was obtained by considering the backing plate, welding speed, and weld power as a parameter. Heat generation during FSP plays a crucial role in controlling the microstructure characteristics and mechanical properties and providing defect-free FSPed materials. As a result, obtaining information regarding peak temperature and thermal history, as well as their interaction with the primary process parameters of FSP, is essential. Proper process parameter settings can provide sufficient heat for recrystallisation, resulting in ultra-fine or fine grain microstructures. Thus, by establishing appropriate process parameters, optimisation plays a critical role in manufacturing high-quality FSP. Many researchers have recently become interested in improving FSP process parameters and have used various optimisation strategies, such as the response surface method[14-15], Taguchi method[16-17] and an artificial neural network to predict the result[18-19].

According to a literature survey, optimisation of process parameters such as rotational speed, traverse speed, tilt angle and especially shoulder diameter against responses such as peak temperature and microhardness is rarely documented. This study aims to optimise the FSP process parameters considering the individual and multi-responses and investigate the factors influencing defect formation and microhardness improvement. Thus, the present work investigates the process parameters using the Taguchi orthogonal array experimental design to fulfil the research gap. The Taguchi-based Grey Relational Analysis (GRA) is utilised for multi-optimisation. The temperature profiles generated during an experimental run are studied and discussed in this paper.

2. EXPERIMENTATION

2.1 Methodology

The material used to investigate surface modification via FSP is aluminium alloy AA6082-T6 having a chemical composition (wt. %) of 0.92 Mg, 0.85 Si, 0.26 Fe, 0.17 Cr, 0.18 Zn, 0.03 Ti, 0.03 Cu and the rest is aluminium. The size of the work plates is cut in a dimension of 200 mm × 50 mm × 8 mm for experimentation. The H13 tool steel is used as a tool material due to its hot hardness and resistance to thermal fatigue cracking. The tool is subsequently hardened to 55 HRC by the heat treatment process. The straight threaded cylindrical pin with concave shoulder end profile tools are used for FSP. The tool shoulder diameter between 16 mm to 25 mm, the effective threaded pin diameter of 6.5 mm (thread pitch: 1 mm),

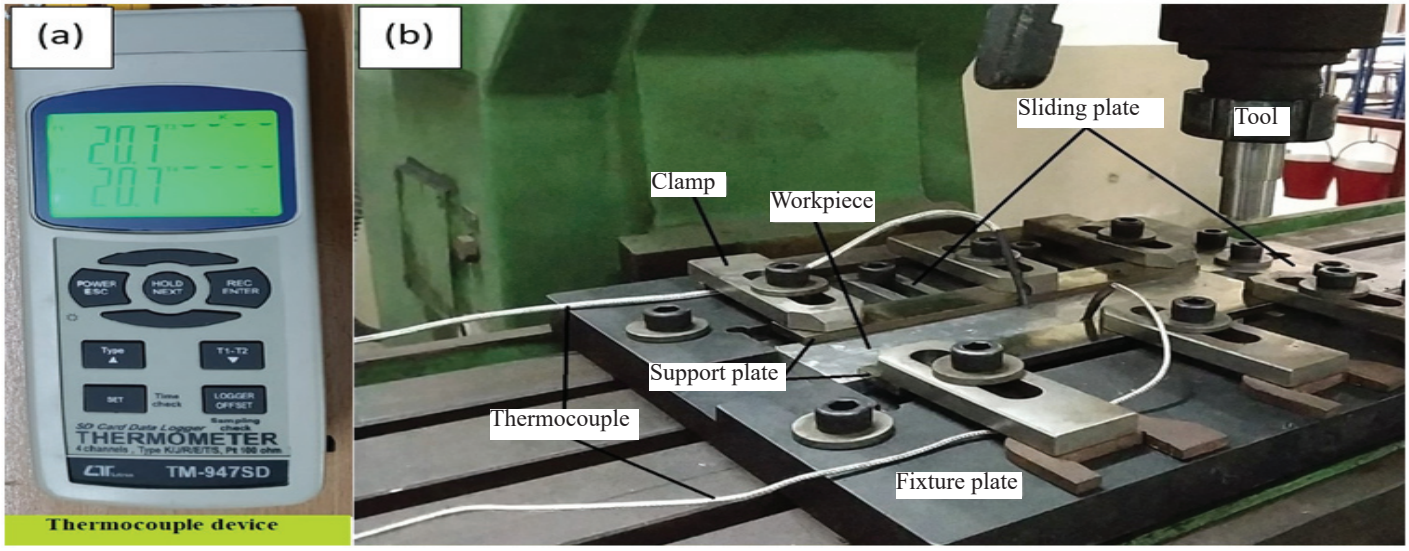

Figure 1. (a) Temperature measuring device; (b)Experimental setup.

and the pin length of 5 mm is considered for tool design. The experiments are performed on a conventional vertical milling machine where the work material is rigidly clamped with the help of a specially designed and manufactured fixture[20] on the milling machine bed, as shown in Fig. 1 (b). Two K-type thermocouples (with a precision of 0.01 ºC) are used to record the temperature history during FSP on the advancing and the retreating side by using a Lutron thermometer (Model: TM-947) as shown in Fig. 1 (a). The T1-AS and T2-RS are the peak temperature notations for the advancing and retreating sides, respectively. The thermocouples with probe diameter 1 mm are inserted in blind holes of 1.5 mm diameter and 4 mm depth on the workpiece at 15 mm away from the centreline on both sides of the processing region. The Vickers microhardness test is performed at the upper region of the stir zone surface using a 200 g indentation load for 10 s and the samples are prepared according to the ASTM E92 standards. For the macrostructure investigation, samples are polished and etched using a 5 % HF solution and observed under an optical microscope.

2.2 Design of experiment

For the present investigation, four process parameters, such as the tool rotational speed (TRS), tool traverse speed (TTS), tool shoulder diameter (TSD), and tool tilt angle (TTA), are selected for the FSP. Peak temperature and microhardness are taken as response variables for the processed region of FSP. The levels of considered process parameters (i.e. "TRS", "TTS", "TSD" and "TTA") are (500, 1000, 1400 ,2000), (20, 40, 80, 112), (16, 19, 22, 25) and (0°, 1°, 2°, 3°) respectively. The range of process parameters is decided by several trial experiments and based on visual inspection of the surface defects and roughness, as explained in the published article[21]. Taguchi L16 orthogonal array is utilised for statistical planning of experiments. This technique is best suited for discrete variables and reduces the number of experiments saving the cost and time of the research[22]. The appropriate orthogonal array choice depends on the interested number of process parameters and their levels[23]. Four process parameters with every three degrees of freedom are taken into account in the current work and thus, there are a total of 12 degrees of freedom. The selected orthogonal array must have a degree of freedom equal to or greater than 12. As a result, L16 is an appropriate orthogonal array as it has 15 degrees of freedom. Thus, the orthogonal arrays are preferred for experimental designs for two reasons: their small size and the fact that they appear to provide satisfactory results for the main effect[24].

The single-pass FSP is considered during experimentation, and the plunge depth is kept as 0.12 mm. Peak temperatures on advancing and retreating sides are recorded during FSP, while microhardness at the stir zone is measured after FSP. Minitab 17.0 is used to choose the orthogonal array and determine the signal-to-noise ratio (S/N ratio) based on response variables. Each experiment is repeated twice and an average is considered to maintain accuracy and determine the S/N ratio. The influence of each process parameter on optimal processing conditions and individual responses are determined using ANOVA. For the multi-response optimisation, S/N ratios of responses 'peak temperature' and 'microhardness' are combined into a single value with the help of GRA and then, the influences of various parameters on responses are determined using ANOVA.

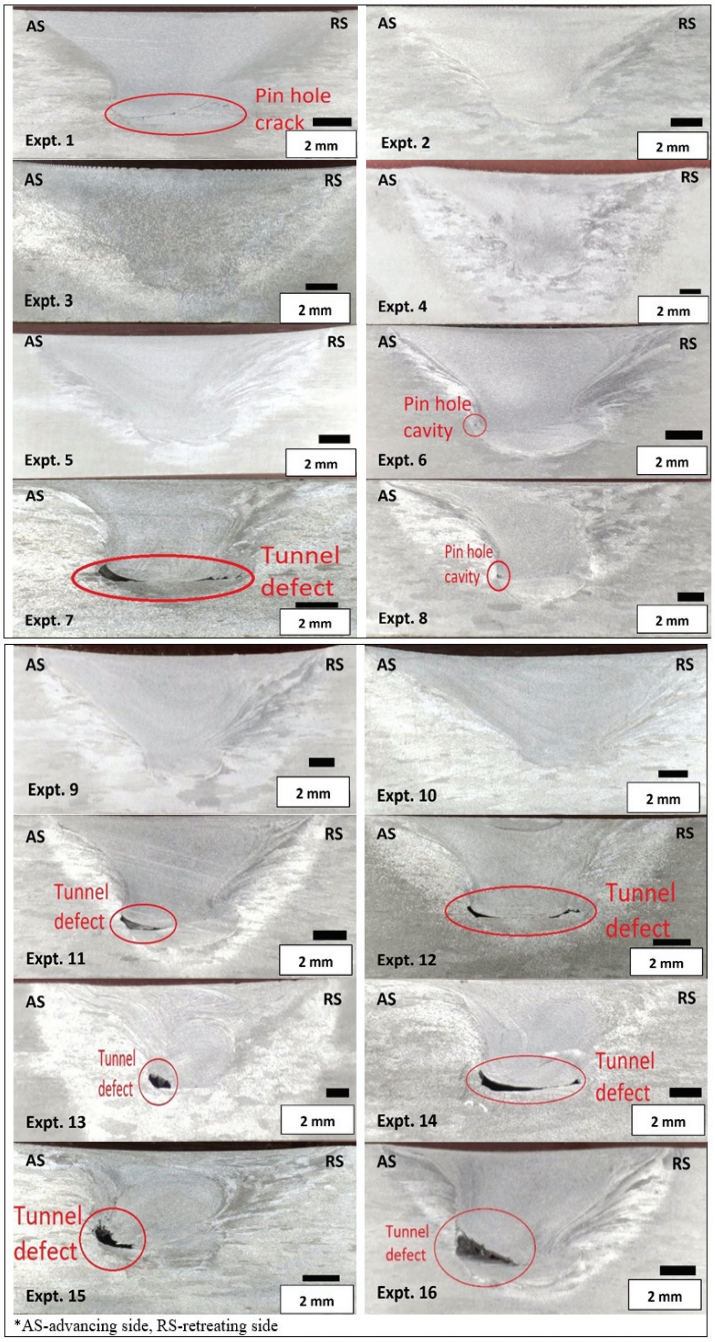

Figure 2. Macrostructure of FSP samples processed region in experimental sequence.

3. RESULTS AND DISCUSSION

3.1 Macro-structure and Defect Formation

The macrographic cross-sectional view of the FSPed AA6082-T6 stir zone with marking is displayed in Fig. 2. There are no visible defects on the upper surface of the processed region in all the post FSPed samples. However, due to insufficient or excessive heat generation and lack of metal consolidation, many defects such as pinholes, cracks and tunnel voids are present within the stirring zone; these observations are consistent with previous researchers[6, 7]. A

significant influence of process parameters is observed from the macroscopic analysis of stir zone shape, size, and defect formation. Almost all the stir zones have inverted trapezoidal shapes due to the extreme deformation and frictional heat. Most of the defects appeared at the corner of the bottom region near the advancing side of the stir zone. This defect occurs when the material fails to merge with the advancing side as it flows from retreating to the advancing side. Also, an abrupt change in the microstructure is visible on the advancing side, while the transition is gradual on the retreating side, which is in line with the previous researchers' work[25].

The formation of defects due to improper process parameters leads to insufficient heat generation[26]. It is observed that with a machine setting of TRS as 2000 rpm, the FSPed samples are defective and a similar condition appears when TSD is 16 mm and/or TTA is 0°, as shown in the cross-section macrostructure of the stir zone (Fig. 2). The higher TRS value (i.e., 2000 rpm) causes excessive heat generation and abnormal stirring, resulting in a discontinuous flow of matrix material, whereas lower TSD (i.e., 16 mm) fails to generate enough heat to support adequate material flow. Further, the 0° TTA and the excessive heat generation due to high TRS squeeze out excessive flash, which reduces matrix material that consolidates in the stir zone. These results are similar to the previously published articles[27-28]. Thus, the main reasons for defect formation are due to excessive heat generation, inadequate heat generation and abnormal stirring[29]. Therefore, it appears that process parameters with the above settings are more probable for defect formation. As shown in Table 1, it is observed that the range of peak temperature from 368 ºC to 476 ºC on the advancing side produced the non-defective FSPed samples, which further validated that the lower and very excessive heat generation is responsible for defect formation. This temperature range is 0.67 to 0.87 times the melting temperature of AA6082-T6, which is usually required to achieve targeted mechanical properties in FSP[1].

Table 1. Peak temperature recorded during FSP experimental sequence

Expt. No.	TRS (rpm)	TTS (mm/min)	TSD (mm)	TTA (degree)	T1-AS (ºC)	T2-RS (ºC)	Hardness (HV)
1	500	20	16	0	311	297	50
2	500	40	19	1	348	335	49
3	500	80	22	2	368	350	63
4	500	112	25	3	385	383	76
5	1000	20	19	2	380	375	48
6	1000	40	16	3	336	311	70
7	1000	80	25	0	339	302	76
8	1000	112	22	1	356	328	79
9	1400	20	22	3	399	400	58
10	1400	40	25	2	476	456	67
11	1400	80	16	1	322	308	73
12	1400	112	19	0	297	274	79
13	2000	20	25	1	503	487	57
14	2000	40	22	0	358	351	69
15	2000	80	19	3	329	312	72
16	2000	112	16	2	330	317	74

3.2 Peak Temperature and Microhardness

During FSP, the peak temperatures are recorded on advancing and retreating sides of the processing region as the rotating tool passes near the thermocouples T1 and T2. It is observed that considered process parameters significantly influenced the peak temperature and microhardness. The frictional force between the tool and the work material increases with the increase in TRS and TSD. Larger the TSD widens the contact area between the tool and the work material. This frictional force is proportionate to heat generation; as a result, peak temperature rises. Thus, TRS and TSD are directly proportional to peak temperature. At higher TTS, limited time is available between tool and work material interaction, leading to lower heat generated and vice-versa. As a result, an increase in TTS is responsible for lower heat generation. This observation is supported by the main effect plot presented in section 3.3.1. For the TTA parameter, contact area and interference between tool and work material significantly influence peak temperature. At a constant plunging depth with lower TTA, the net effect of lower interference and large contact area give rise to the temperature. After a certain higher value of TTA, the temperature reduces as less contact area is available to generate frictional heat.

The temperature profile consists of heating and cooling rates. The variations in cycle time (i.e., total heating and cooling time) are responsible for the change in mechanical and microstructural properties of FSPed samples[9]. A longer cycle time allows more heat generation during FSP causes grain coarsening, whereas a shorter cycle time provides lower heat for grain growth and freezes into a fine-grain microstructure, resulting in good mechanical properties. The temperature profiles generated during experimental runs at 2000 rpm are displayed in Fig. 3(a). The plots clearly depict that the increase in TTS decreases the cycle time and hence corresponding peak temperature decreases due to lower heat generation. Furthermore, the temperature profiles show that temperature distribution is asymmetric from the centre of the stir zone line as the temperature on the advancing side is higher than a retreating side, which is consistent with the previous researchers' work[9, 12]. The relative motion between the tool shoulder and the work material interface is higher on the advancing side than on the retreating side, leading to a greater strain rate, escalating plastic deformation and heat generation on the advancing side[30].

Figure 3(b) shows the Vickers microhardness indentation at the stir zone of FSPed AA6082-T6. A strong correlation between TTS and microhardness is observed, which is further corroborated in the following sections using statistical analysis. As mentioned above, lower cycle time means lower heat generation that inhibits grain growth during dynamic recrystallisation, which results in higher microhardness. Thus, better microhardness is obtained at the higher TTS due to lower cycle time. However, defect formation problems like tunnelling or voids are most likely to occur at a lower temperature as the flowability of plastically deformed material gets reduced[31],

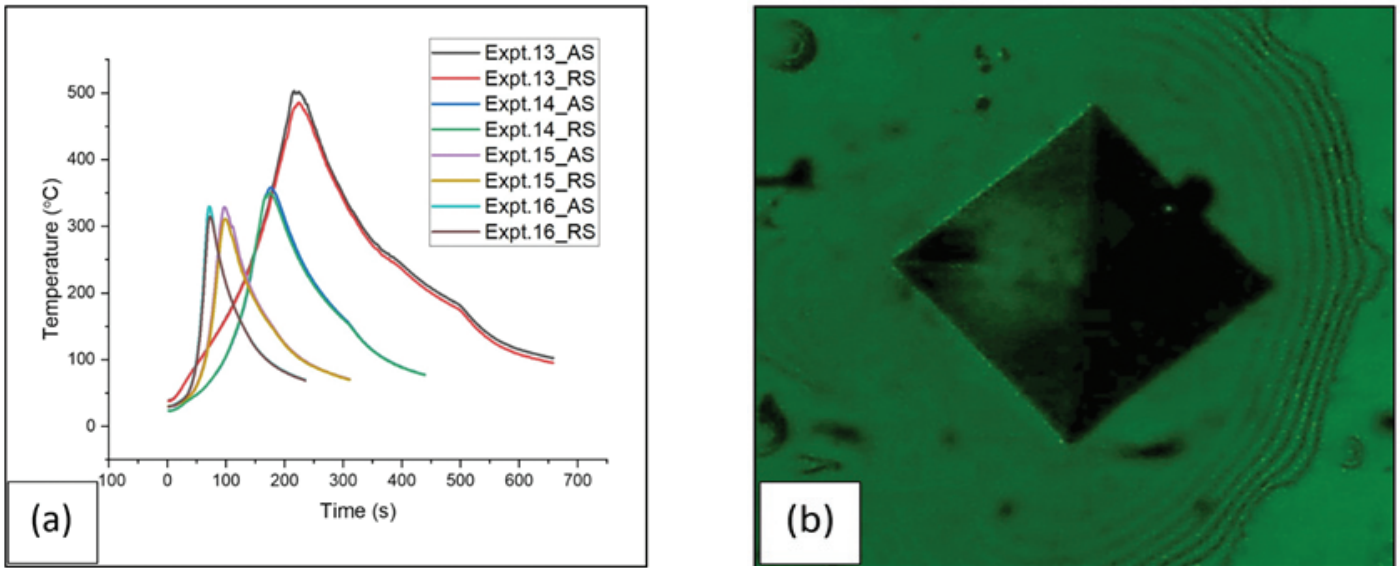

Figure 3. (a) Temperature profiles recorded during FSP at 2000 rpm (b) microhardness indentation pattern at stir zone.

which can be adjusted by a slight increase in TTA (i.e., 1° - 2°) for proper material consolidation in stir zone[32-33].

3.3 Statistical Analysis

Experiments are conducted in random order and their measured responses are shown in Table 2. The maximum defect occurs at lower temperatures as observed from the macrostructure study due to which material fails to flow plastically, leading to poor stir zone consolidation. Thus, the present study aims to retain the peak temperature as high as possible to avoid defect formation. Therefore, "higher-the-better" is considered for peak temperature[9] and microhardness (Eqn. 1).

$$\frac{S}{N} = -10\log\left(\frac{1}{n}\sum_i^n \frac{1}{y_i^2}\right) \text{ (for "higher-the-better")} \quad (1)$$

Where y_i is the value of the response variable of the i^{th} test, and n is the number of replications.

Table 2. Sequence of S/N values for the responses T1-AS, T2-RS, and microhardness

Expt. No.	S/N ratio (T1-AS)	S/N ratio (T2-RS)	S/N ratio (Microhardness)
1	49.855	49.455	33.891
2	50.819	50.488	33.798
3	51.317	50.868	35.917
4	51.698	51.653	37.554
5	51.584	51.469	33.532
6	50.514	49.841	36.839
7	50.591	49.586	37.558
8	51.017	50.317	37.897
9	52.009	52.030	35.192
10	53.543	53.170	36.456
11	50.144	49.757	37.206
12	49.440	48.739	37.897
13	54.023	53.742	35.040
14	51.065	50.894	36.713
15	50.331	49.883	37.085
16	50.370	50.007	37.325

3.3.1 Individual Response Optimisation

The S/N ratio of the main effect plot is shown in Fig. 4, which indicates the optimal conditions and influences of process parameters on response factor T1-AS, T2-RS, and microhardness. The higher the S/N ratio, the higher is the quality; thus, an increase in TRS or TSD raises the peak temperature while a decrease in TTS lowers the peak temperature. TTA increases peak temperature to a specific limit and then drops with TTA. Thus, the peak temperature (T1-AS and T2-RS) have an optimal level setting as TRS of 2000 rpm, TTS of 20 mm/min, TSD of 25 mm, and TTA of 2°. Likewise, the main effect plot of microhardness inferred that an increase in TRS up to a certain limit improves microhardness, which declines in proportion to TRS. The decrease in TSD to a certain level reduces microhardness; after that, it increases with respect to TSD and a similar phenomenon is observed in TTA. In contrast, an increase in TTS decreases microhardness. Thus, the optimal condition for the microhardness is obtained at TRS of 1400 rpm, TTS of 112 mm/min, TSD of 25 mm, and TTA of 3°.

The ANOVA result for peak temperature (T1-AS and T2-RS) and hardness are shown in Table 3. A higher value of F (i.e., F-distribution) signifies the more significant impact on the response variable. It can be observed that TSD has the maximum impact (52.19 %) on peak temperature T1-AS, followed by TTA (21.95 %), TTS (20.96 %), and TRS (3.62 %). Similarly, in the case of T2-RS, TSD has a maximum

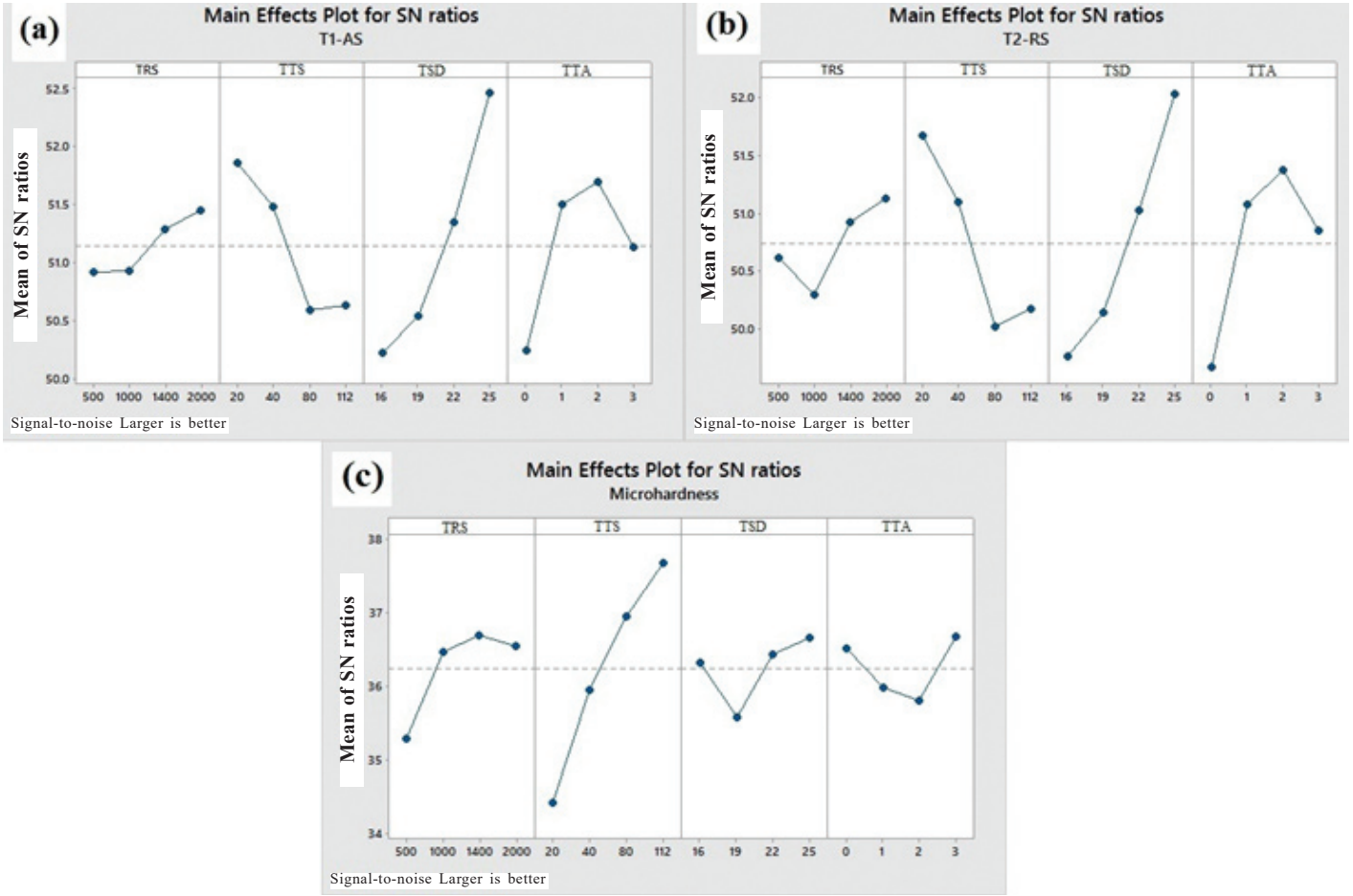

Figure 4. Main effects plot for (a) T1-AS, (b) T2-RS and (c) microhardness.

Table 3. ANOVA for individual response T1-AS, T2-RS, and microhardness

	Factors	Adj SS	DOF	Variance	F- Test	% Contribution
T1-AS	TRS	0.83	3	0.28	2.84	3.62
	TTS	4.82	3	1.61	16.45	20.96
	TSD	11.99	3	4.00	40.97	52.19
	TTA	5.04	3	1.68	17.23	21.95
	Error	0.29	3	0.10		1.27
	Total	22.98	15	1.53		100.00
T2-RS	TRS	1.57	3	0.52	4.33	5.56
	TTS	7.31	3	2.44	20.16	25.88
	TSD	12.28	3	4.09	33.86	43.47
	TTA	6.73	3	2.24	18.54	23.80
	Error	0.36	3	0.12		1.28
	Total	28.26	15	1.88		100.00
Microhardness	TRS	4.96	3	1.65	10.71	14.65
	TTS	23.80	3	7.93	51.39	70.28
	TSD	2.60	3	0.87	5.61	7.67
	TTA	2.04	3	0.68	4.41	6.03
	Error	0.46	3	0.15		1.37
	Total	33.86	15	2.26		100.00

impact (43.47 %), followed by TTS (25.88 %), TTA (23.80 %), and TRS (5.56 %). For microhardness, TTS has a maximum impact (70.28 %), followed by TRS (14.65 %), TSD (7.67 %), and TTA (6.03 %).

3.3.2 Multi Response Optimisation

For multi-objective functions, the Taguchi method is not enough; thus, GRA integrated with Taguchi is used for further analysis. The S/N ratios of responses (i.e., peak temperature and microhardness) are first normalised between 0 and 1 using the formula "higher-the-better" (Eqn. 2). The associating normalised S/N ratios are then converted into Grey relational coefficient[34] (GRC), computed using Eqn. 3.

For higher the better,

$$Z_{ij} = \frac{\left(Y_{ij} - \min Y_{ij}\left(i = 1,2,...n\right)\right)}{\left(\max Y_{ij}\left(i = 1,2,...n\right) - \min Y_{ij}\left(i = 1,2,...n\right)\right)} \quad (2)$$

Where, Z_{ij} is the normalised value of an i^{th} experiment for a j^{th} dependent response for "higher-the-better" values.

$$\xi_{ij} = \frac{\Delta_{\min} + \lambda\Delta_{\max}}{\Delta_i\left(k\right) + \lambda\Delta_{\max}} \quad (3)$$

Where, ξ_i is the GRC for i^{th} experiment and j^{th} is a dependent variable, Δ is a notation of absolute difference

Table 4. Computation of GRG and Rank

Expt. No.	Normalized value		Δ		GRC		GRG	Rank
	T1-AS	Micro-hardness	T1-AS	Micro-hardness	T1-AS	Micro-hardness		
1	0.09	0.08	0.91	0.92	0.355	0.352	0.353	16
2	0.30	0.06	0.70	0.94	0.417	0.347	0.382	15
3	0.41	0.53	0.59	0.47	0.459	0.514	0.486	13
4	0.49	0.89	0.51	0.11	0.496	0.817	0.657	4
5	0.47	0.00	0.53	1.00	0.484	0.333	0.409	14
6	0.23	0.73	0.77	0.27	0.395	0.650	0.522	11
7	0.25	0.89	0.75	0.11	0.400	0.819	0.609	6
8	0.34	0.96	0.66	0.04	0.433	0.933	0.683	3
9	0.56	0.37	0.44	0.63	0.532	0.441	0.487	12
10	0.90	0.65	0.10	0.35	0.827	0.585	0.706	2
11	0.15	0.81	0.85	0.19	0.371	0.726	0.549	8
12	0.00	0.96	1.00	0.04	0.333	0.933	0.633	5
13	1.00	0.33	0.00	0.67	1.000	0.428	0.714	1
14	0.35	0.70	0.65	0.30	0.437	0.627	0.532	10
15	0.19	0.78	0.81	0.22	0.383	0.699	0.541	9
16	0.20	0.84	0.80	0.16	0.385	0.755	0.570	7

Table 5. Response table for GRG

LEVEL	TRS	TTS	TSD	TTA
1	0.470	0.491	0.499	0.532
2	0.556	0.536	0.491	0.582
3	0.594	0.546	0.547	0.543
4	0.589	0.636	0.672	0.552

Table 6. ANOVA for GRG

Factors	Adj SS	DOF	Variance	F- Test	% Contribution
TRS	0.040	3	0.013	2.80	21.23
TTS	0.044	3	0.015	3.12	23.62
TSD	0.084	3	0.028	5.89	44.62
TTA	0.006	3	0.002	0.39	2.95
Error	0.014	3	0.005		7.58
Total	0.187	15	0.012		100.00

among the Y_{oj} and Y_{ij} that can address as a quality loss (Eqn. 3). Y_{oj} is the best-normalised value of the j^{th} response, Y_{ij} is the i^{th} normalised value of the j^{th} dependent variable, and λ is the distinguished coefficient $(0 \le \lambda \le 1)$. The acknowledgement of λ value is based on the requirements of the practical system[34]. In the present study, the value[35] of λ for peak temperature T1-AS and microhardness is taken as 0.5.

The final step is to evaluate the Grey relational grade (GRG) using Eqn. 4.

Table 7. Confirmation test for peak temperature and microhardness

Performance parameter	Level	Predicted	Experimental
T1-AS (ºC)	$TRS_{level-4}$ $TTS_{level-1}$ $TSD_{level-4}$ $TTA_{level-3}$	497.8	493.7
T2-RS (ºC)	$TRS_{level-4}$ $TTS_{level-1}$ $TSD_{level-4}$ $TTA_{level-3}$	490.1	483.3
Microhardness (HV)	$TRS_{level-3}$ $TTS_{level-4}$ $TSD_{level-4}$ $TTA_{level-4}$	84.9	81.0

$$GRG = \frac{1}{m}\sum_{j=1}^{m} \xi_{ij} \quad (4)$$

Where, m is the total number of response factors.

The computed GRG values are noted in Table 4. A higher value of GRG indicates an optimal condition for quality characteristics. Table 5 shows the optimal TRS of 1400 rpm, the TTS of 112 mm/min, TSD of 25 mm, and TTA of 1°. The ANOVA result of Table 6 indicates that TSD has a maximum impact (44.62 %), followed by TTS (23.62 %), TRS (21.23 %), and TTA (2.95 %).

Table 8. Confirmation test for GRA

Response	Parameters in the thirteenth trail ($TRS_{level-4}$, $TTS_{level-1}$, $TSD_{level-4}$, $TTA_{level-2}$)	Optimum parameters	
		Predicted ($TRS_{level-3}$, $TTS_{level-4}$, $TSD_{level-4}$, $TTA_{level-2}$)	Experimental ($TRS_{level-3}$, $TTS_{level-4}$, $TSD_{level-4}$, $TTA_{level-2}$)
T1-AS (ºC)	503	-	425
T2-RS (ºC)	487	-	404
Microhardness (HV)	57	-	80
GRG	0.714	0.827	0.806

3.3.3 Confirmation Test

The confirmatory tests are conducted to approve the analysis of experimental results. The optimum condition obtained from response tables is the same for T1-AS and T2-RS. It is at level-4 for TRS, level-1 for TTS, level-4 for TSD, and level-3 for TTA. For microhardness, the optimal condition is level-3 for TRS, level-4 for TTS, level-4 for TSD, and level-4 for TTA. The prediction of these optimal levels is calculated using Eqn. 5.

$$\eta_{predicted} = T\sum\left(\eta_i - T\right) \quad (5)$$

Where T is the overall mean of a process parameter, η_i is the average value of a significant parameter. The predicted S/N ratio of response factors T1-AS, T2-RS, and microhardness are as follows.

$$\left(T1-AS\right)\eta_{predicted} = TRS_{level-4} + TTS_{level-1} + TSD_{level-4} + TTA_{level-3} - 3T = 497.8°C$$

$$\left(T2-RS\right)\eta_{predicted} = TRS_{level-4} + TTS_{level-1} + TSD_{level-4} + TTA_{level-3} - 3T = 490.1°C$$

$$\left(Microhardness\right)\eta_{predicted} = TRS_{level-3} + TTS_{level-4} + TSD_{level-4} + TTA_{level-4} - 3T = 84.9HV$$

Where TRS, TTS, TSD, and TTA are the average value of the S/N ratio at the considered process parameter's level. Similarly, the prediction of GRG value can be calculated as follow.

$$\left(GRG\right)\eta_{predicted} = TRS_{level-3} + TTS_{level-4} + TSD_{level-4} + TTA_{level-2} - 3T = 0.827$$

As shown in Table 7 for individual response variables, the experimental results are found within the confidence interval. From Table 8, when experimental results are at the optimum level compared with the thirteenth experimental trial (which has the first rank), GRG has been enhanced by 0.092. Hence it is feasible to state that the Taguchi-based GRA is a convenient tool for optimizing multi-response parameters like peak temperature and microhardness.

4. CONCLUSION

In this paper, the friction stir processing parameters (i.e., TRS, TTS, TSD, and TTA) for processing the aluminium alloy AA6082-T6 are optimised against the responses 'peak temperature' and 'microhardness' using Taguchi GRA. With the considered levels of the process parameters for the same working material and tool dimensions, defect-free samples are found when the peak temperature range of the advancing side varies from 368 ºC to 476 ºC. The TSD and the TRS are directly proportional, while the TTS is inversely proportional to the peak temperature. Higher TTS results in lower peak temperature and thus, a higher microhardness value is achieved.

In the case of single response optimisation, the optimal combination of process parameters obtained for peak temperature is TRS: 2000 rpm, TTS: 20 mm/min, TSD: 25 mm and TTA: 2°. The TSD has the highest percentage contribution for peak temperature (i.e., 52.19% for T1-AS and 43.47% for T2-RS). The values of peak temperature on the advancing and retreating sides obtained are 493.7 ºC and 483.3 ºC, respectively. An optimal combination of process parameters obtained for microhardness is TRS: 1400 rpm, TTS: 112 mm/min, TSD: 25 mm and TTA: 3°. The TTS has the highest percentage contribution for microhardness (i.e., 70.28 %). The value of microhardness obtained is 81.0 HV.

In the case of multi-response optimisation, the optimal condition obtained for both peak temperature and microhardness is TRS: 1400 rpm, TTS: 112 mm/min, TSD: 25 mm and TTA: 1º. The TSD has the highest percentage contribution (i.e., 44.62 %) on the performance parameters. The peak temperatures on the advancing and retreating sides are 425°C and 404°C, respectively. The microhardness value obtained is 80 HV. These values are the trade-off between peak temperature and microhardness.

Thus, the Taguchi-based GRA method has proved its applicability for solving the multi-response optimisation problem in the FSP process. The findings of current research are helpful to manufacturing practitioners in selecting the optimal parameters for defect-free stir zone in the FSP process to obtain desired responses.

REFERENCES

1. Mishra, R.S. & Ma, Z.Y. Friction stir welding and processing. *Mater. Sci. Eng. R. Reports.*, 2005, **50**(1–2), 1–78. doi: 10.1016/j.mser.2005.07.001.
2. Bhoi, N.K.; Singh, H. & Pratap, S. Developments in the aluminum metal matrix composites reinforced by micro/nano particles – A review. *J. Compos. Mater*., 2020, **54**(6), 813–833. doi: 10.1177/0021998319865307.
3. Premnath, A. Optimisation of the process parameters on the mechanical and wear properties of Al-SiC Nano-Composites fabricated by friction stir processing using desirability approach. *Silicon*., 2020, **12**(3), 665–675. doi: 10.1007/s12633-019-00178-6.
4. Patel, V.; Li, W.; Vairis, A. & Badheka, V. Recent development in friction stir processing as a solid-state grain refinement technique: Microstructural evolution and

property enhancement. *Crit. Rev. Solid State Mater. Sci*., 2019, **44**(5), 378–426.
doi: 10.1080/10408436.2018.1490251.

5. Rajeshkumar, R.; Udhayabanu, V.; Srinivasan, A. & Ravi, K.R. Microstructural evolution in ultrafine grained Al-Graphite composite synthesized via combined use of ultrasonic treatment and friction stir processing. *J. Alloys Compd*., 2017, **726**, 358–366.
doi: 10.1016/j.jallcom.2017.07.280.
6. Vijayavel, P.; Balasubramanian, V. & Sundaram, S. Effect of shoulder diameter to pin diameter (D/d) ratio on tensile strength and ductility of friction stir processed LM25AA-5% SiCp metal matrix composites. *Mater. Des*., 2014, **57**, 1–9.
doi: 10.1016/j.matdes.2013.12.008.
7. Elangovan, K. & Balasubramanian, V. Influences of pin profile and rotational speed of the tool on the formation of friction stir processing zone in AA2219 aluminium alloy. *Mater. Sci. Eng. A*., 2007, **459**(1–2), 7–18.
doi: 10.1016/j.msea.2006.12.124.
8. Patel, V.; Badheka, V.; Li, W. & Akkireddy, S. Hybrid friction stir processing with active cooling approach to enhance superplastic behavior of AA7075 aluminum alloy. *Arch. Civ. Mech. Eng*., 2019, **19**(4), 1368–1380.
doi: 10.1016/j.acme.2019.08.007.
9. Chaudhary, B.; Patel, V.; Ramkumar, P.L. & Vora, J. Temperature distribution during friction stir welding of AA2014 aluminum alloy: Experimental and statistical analysis. *Trans. Indian Inst. Met*., 2019, **72**(4), 969–981.
doi: 10.1007/s12666-018-01558-z.
10. Wahid, M.A.; Khan, Z.A.; Siddiquee, A.N.; Shandley, R. & Sharma, N. Analysis of process parameters effects on underwater friction stir welding of aluminum alloy 6082-T6. *Proc. Inst. Mech. Eng. Part B J. Eng. Manuf*., 2019, **233**(6), 1700–1710.
doi: 10.1177/0954405418789982.
11. Yousefpour, F.; Jamaati, R. & Aval, H.J. Effect of traverse and rotational speeds on microstructure, texture, and mechanical properties of friction stir processed AZ91 alloy. *Mater. Characterization,* 2021, 111235.
doi: 10.1016/j.matchar.2021.111235.
12. Cartigueyen, S. & Mahadevan, K. Effects of thermal conditions on microstructure and mechanical properties of Cu–SiCp Surface nanocomposites by friction stir processing route. *Trans. Indian Inst. Met*., 2019, **72**(2), 289–305.
doi: 10.1007/s12666-018-1480-z.
13. Stringham, B.J.; Nelson, T.W. & Sorensen, C.D. Non-dimensional modeling of the effects of weld parameters on peak temperature and cooling rate in friction stir welding. *J. Mater. Process. Technol*., 2018, **255**, 816–830.
doi: 10.1016/j.jmatprotec.2017.11.044.
14. Verma, S.; Garg, D.; Misra, J.P. & Batra, U. Multi-objective optimum design for FS welded 7039 aluminium alloy considering weld quality issues. *Mater. Today Commun.*, 2021, **26**, 102010.
doi: 10.1016/j.mtcomm.2021.102010.
15. Chakradhar, D. & Narendranath, S. Analysis of the Effect of Friction Stir Welding Parameters on Characteristics of AA6061 Composites using Response Surface Methodology. *Trans. Indian Inst. Met.*, 2021, 1-17.
doi: 10.1007/s12666-021-02214-9.
16. Maji, P.; Nath, R.K.; Karmakar, R.; Madapana, D.; Meitei, R.K. & Ghosh, S.K. Wear and corrosion behavior of Al7075 matrix hybrid composites produced by friction stir processing: Optimization of process parameters. *JOM*, 2021, 1-13.
doi: 10.1007/s11837-021-04945-y.
17. Prasad, K.A. & John, M.S. Optimisation of external roller burnishing process on magnesium silicon carbide metal matrix composite using response surface methodology. *J. Brazilian Soc. Mech. Sci. Engin.*, 2021, **43**(7), 1-12.
doi: 10.1007/s40430-021-03069-3.
18. Jamalian, H.M.; Eskandar, M.T.; Chamanara, A.; Karimzadeh, R. & Yousefian, R. An artificial neural network model for multi-pass tool pin varying FSW of AA5086-H34 plates reinforced with Al2O3 nanoparticles and optimization for tool design insight. CIRP *J. Manuf. Sci. Technol.*, 2021, **35**, 69-79.
doi: 10.1016/j.cirpj.2021.05.007.
19. Verma, S., Misra; J.P.; Singh, J.; Batra, U. & Kumar, Y. Prediction of tensile behavior of FS welded AA7039 using machine learning. *Mater. Today Commun.*, 2021, **26**, 101933.
doi: 10.1016/j.mtcomm.2020.101933.
20. Sarvaiya, J. & Singh, D. Design and development of robust fixture to perform friction stir welding/processing on conventional vertical milling machine. *In* Advances in Manufacturing Systems: Select Proceedings of RAM 2020, 2021, **83**.
doi: 10.1007/978-981-33-4466-2_9.
21. Sarvaiya, J. & Singh, D. Determination of defect-free working range of friction stir processing for AA6082-T6. *In* Recent Advances in Smart Manufacturing and Materials, Springer*,* 2021, 327–339.
22. Montgomery, D.C. Design & analysis of experiments. John wiley & sons, 2017.
23. Pannerselvam, R. Design & analysis of experiments. PHI Learning Pvt. Ltd., 2012.
24. Tamizharasan, T.; Senthilkumar, N.; Selvakumar, V. & Dinesh, S. Taguchi's methodology of optimizing turning parameters over chip thickness ratio in machining P/M AMMC. *SN Appl. Sci.*, 2019, **1**(2), 160.
doi: 10.1007/s42452-019-0170-8.
25. Sharma, V.; Prakash, U. & Kumar, B.V.M. Surface composites by friction stir processing: A review. *J. Mater. Process. Technol*., 2015, **224**, 117–134.
doi: 10.1016/j.jmatprotec.2015.04.019.
26. Akbari, M.; Aliha, M.R.M.; Keshavarz, S.M.E. & Bonyadi, A. Effect of tool parameters on mechanical properties, temperature, and force generation during FSW. *Proc. Inst. Mech. Eng. Part L J. Mater. Des. Appl*., 2019, **233**(6), 1033–1043.
doi: 10.1177/1464420716681591.
27. Mehta, K.P. & Badheka, V.J. Effects of tilt angle on the properties of dissimilar friction stir welding copper to

aluminum. *Mater. Manuf. Processes*, 2016, **31**(3), 255–263.
doi: 10.1080/10426914.2014.994754.
28. Zhai, M.; Wu, C. & Su, H. Influence of tool tilt angle on heat transfer and material flow in friction stir welding. *J. Manuf. Processes*, 2020, **59**, 98–112.
doi: 10.1016/j.jmapro.2020.09.038.
29. Dialami, N., Cervera, M., & Chiumenti, M. Defect formation and material flow in friction stir welding. *Eur. J. Mech. -A/Solids*, 2020, **80**, 103912.
doi: 10.1016/j.euromechsol.2019.103912.
30. Ansari, M.A.; Samanta, A.; Behnagh, R.A. & Ding, H. An efficient coupled Eulerian-Lagrangian finite element model for friction stir processing. *Int. J. Adv. Manuf. Technol*., 2019, **101**(5), 1495–1508.
doi: 10.1007/s00170-018-3000-z.
31. Bharti, S.; Ghetiya, N.D. & Patel, K.M.A review on manufacturing the surface composites by friction stir processing. *Mater. Manuf. Processes*, 2021, **36**(2), 135-170.
doi: 10.1080/10426914.2020.1813897.
32. Meshram, S.D. & Reddy, G.M. Influence of Tool Tilt Angle on Material Flow and Defect Generation in Friction Stir Welding of AA2219. *Def. Sci. J.*, 2018, **68**(5).
doi: 10.14429/dsj.68.12027.
33. Sharifitabar, M.; Sarani, A.; Khorshahian, S. & Afarani, M.S. Fabrication of 5052Al/Al2O3 nanoceramic particle reinforced composite via friction stir processing route. *Mater. Des.*, 2011, **32**(8-9), 4164–4172.
doi: 10.1016/j.matdes.2011.04.048.
34. Kumari, N.; Gohel, J.V. & Patel, S.R. Multi-response optimization of ZnO thin films using Grey-Taguchi technique and development of a model using ANN. Optik, 2017, **144**, 422–435.
doi: 10.1016/j.ijleo.2017.06.107.
35. Prakash, K.S.; Gopal, P.M. & Karthik, S. Multi-objective optimization using Taguchi based grey relational analysis in turning of Rock dust reinforced Aluminum MMC. *Meas.*, 2020, **157**, 107664.
doi: 10.1016/j.measurement.2020.107664.

CONTRIBUTORS

Mr Jainesh Sarvaiya obtained his MTech in Manufacturing System Engineering from MNIT Jaipur, India. His area of interest is fabrication of surface composites using friction stir processing.
In current study, he performed the experiments, carried out testing, analysed the experimental data and contributed in writing of the research paper.

Dr Dinesh Singh obtained his PhD (Mechanical Engineering) from Sardar Vallabhbhai National Institute of Technology, Surat. He is working as an Assistant Professor in the Department of Mechanical Engineering, Sardar Vallabhbhai National Institute of Technology, Surat, India. His research interests include advanced manufacturing technology, production and operations management, non-traditional optimisation techniques and multiple attribute decision making techniques in manufacturing environment.
In the current study, he encouraged for the present conducted research work, analysed the experimental data by proposed methodology and given the shape of research paper in present form. He revised the manuscript based on the reviewer's comments.